IEEE Access
Multidisciplinary | Rapid Review | Open Access Journal

IEEE POWER & ENERGY SOCIETY SECTION

Received 3 May 2023, accepted 22 May 2023, date of publication 8 June 2023, date of current version 15 June 2023.

Digital Object Identifier 10.1109/ACCESS.2023.3281562

RESEARCH ARTICLE

Optimal Energy Dispatch Engine for PV-DG-ESS Hybrid Power Plants Considering Battery Degradation and Carbon Emissions

LAITH KANAAN, (Graduate Student Member, IEEE), LOAY S. ISMAIL, (Senior Member, IEEE), SAMER GOWID, (Senior Member, IEEE), NADER MESKIN, (Senior Member, IEEE), AND AHMED M. MASSOUD, (Senior Member, IEEE)

Department of Electrical Engineering, Qatar University, Doha, Qatar

Corresponding author: Laith Kanaan (Kanaan@IEEE.org)

This work was supported by Qatar University and Sultan Qaboos University under Grant IRCC-2022-609.

ABSTRACT Uncertainties in load and solar power forecasting, complex energy storage system (ESS) constraints, and feedback correction pose challenges for very short-term and short-term hybrid power plant scheduling. This paper proposes a two-stage mixed-integer linear programming (MILP)-based energy dispatch engine (EDE). The proposed model ensures optimized scheduling through accurate load and power forecasting, a feedback correction loop, and a set of constraints governing the state of charge (SOC) and state of health (SOH) of the ESS. Such an EDE aims to reduce the plant's operating costs and the usage of diesel generators (DGs), and minimize the cost of carbon emissions. To test the performance of the developed model, real-time load and photovoltaic (PV) data were used in conjunction with a PV-DG-ESS hybrid plant. The system was evaluated against a heuristic control model and a multistage stochastic control model, with the daily overall electricity and carbon emission costs as evaluation metrics. The test results revealed a 9.2% and 3.5% decrease in daily costs compared to the heuristic and stochastic methods, respectively, and a 29.4% decrease in carbon emission costs.

INDEX TERMS Hybrid power plants, energy management system (EMS), energy dispatch engine (EDE), mixed integer linear programming (MILP), optimization, forecasting.

I. INTRODUCTION

The energy consumption rates have increased exponentially over the last few decades. Until recently, this energy demand was met by conventional energy resources (i.e., natural gas and oil), which severely impact the environment by producing greenhouse gases [1]. Renewable energy sources (RESs) and energy storage systems (EESs) in hybrid power plants have grown tremendously to produce a clean energy footprint. An energy management system (EMS) can be used to ensure full utilization of RESs while maximizing plant profits.

EMSs are defined as systems that can achieve effective and optimal operation of distributed energy resources (DERs) at a minimum cost, as per the International Electro-Technical Commission's (IEC) standard IEC-61.970 [2]. They generally consist of three processes: analytics, forecasting, and optimization. EMSs serve as a link between the DERs, ESSs, and load, where the EMS controls the charging and discharging process of the ESSs, manages the use of fossil-based energy generators, and optimally schedules the available resources.

An EMS can manage such operations using three main control schemes: centralized, decentralized, and distributed. A centralized EMS control consists of multiple local controllers responsible for collecting data sent to the main controlling unit through end-to-end communication protocols [3]. Although this method is easier to control, it is inefficient because the slow response time is proportional to the deployment area, rendering it infeasible. Decentralized EMS control involves multiple control units collaborating

The associate editor coordinating the review of this manuscript and approving it for publication was Pratyasa Bhui.

by exchanging data to finalize the global decisions for all nodes [4]. Distributed EMS control is a mixture of centralized and decentralized approaches, where local nodes use their data and data from neighboring nodes to help the centralized node reach an optimal global solution for the system [5].

Forecasting data is an integral block of EMSs because it creates a larger set of analyzable data, including electricity prices, weather data, RESs generation data, and load profiles. Forecasting in an EMS can be categorized based on the forecast period [6].

Very short-term forecasts usually range from a few seconds to half an hour, and are used to perform micro-adjustments on RESs in response to changes in demand. Short-term forecasts typically range from half an hour to 24 hours, and are used for scheduling purposes between RESs and ESSs. Long-term forecasts range from a day to a week, and are used in price forecasting and load scheduling [7].

Another method of classifying forecasting algorithms in EMSs is the model used, where the forecast can either be based on a linear model, such as time-series, State Space, autoregressive moving average (ARMA), and others, or a nonlinear model, including support vector machine (SVM), Markov reward, stochastic programming, fuzzy logic, convoluted neural networks (CNN), and long short-term memory (LSTM).

Although load forecasting can be performed using previous data, it is essential to categorize loads to achieve an accurate forecast. Controllable loads are loads controlled by the plant operator in proportion to the pool prices. Meanwhile, shiftable loads can be shifted over time to achieve a better demand response, such as charging electric vehicles, kitchen appliances, and heavy machinery [8].

After the data are processed, and necessary data are forecasted, the EMS optimizes the use of power by considering certain constraints. These techniques can be classified into three categories according to their complexity: intelligent, metaheuristic, and classical.

Intelligent methods utilize fuzzy logic or neural networks to optimize the power transfer through a set of weights attached to variables in a computing network [9]. Although this method yielded the most optimized results, it was computationally intensive.

Metaheuristic methods use random search and simulation algorithms such as Monte Carlo simulations to maximize or minimize an objective function with or without set constraints [10]. This method includes, but not limited to, particle swarm optimization (PSO), genetic algorithm (GA), and grey-wolf optimization (GWO). Although this method is not as computationally extensive as the intelligent one, it requires a considerably longer time to solve the optimization problem.

Classical methods are characterized by their classical/mathematical nature, where the objective is to maximize or minimize an objective function for a set of constraints. It can be based on initial values and set parameters, as is the case for linear and nonlinear programming (LP/NLP) and mixed-integer linear and nonlinear programming (MILP/MINLP), or it is based on an element of randomness added to the model, such as dynamic programming (DP) and stochastic programming (SP) [11].

To solve the energy dispatch problem, a model predictive control (MPC)-based rolling optimization with feedback correction was proposed in [12] and [13]. While the ESS in [12] and [13] had constraints related to its state of charge (SOC), it lacked state of health (SOH) constraints, which would result in substantial overhead losses when using the model in a realistic system owing to battery degradation. It is also worth noting that the method proposed in [12] and [13] does not specify a local forecasting algorithm, making the forecasted signals unrealistic and impractical compared with the locally forecasted power and load profiles. Similarly, the authors in [14] presented a stochastic MPC model for ESS dispatch. However, they suffer from the same issues as those in [12] and [13] in terms of forecasting and constraints. Another approach combines multistage stochastic optimization and rule-based control [15], where uncertainties are accounted for. However, the forecasting method used in [15] is computationally extensive and time-consuming, making it infeasible for real-time applications. The management of hybrid renewable energy sources, including ESS, was addressed in [16], with improved forecasting of wind and solar outputs through weather forecasting based on deep neural networks. However, previous weather data were not utilized in the training process, and the effect of forecasting uncertainties, modeled through a Gaussian distribution curve, on the optimized output, remains untested. In [17], a discrete-time Markov process model was proposed to optimally operate a photovoltaic (PV)-ESS plant. The authors of [18] presented a similar approach for smoothing RESs power generation. Owing to the use of a statistical tool, such as the Markov reward process, as well as ramp rate control algorithms, the predictions made in [17] and [18] are viable only for short-term forecasting (minutes at most). A multilayer MPC-based approach, which modeled the battery and supercapacitor degradation, was considered in [19]. However, the uncertainties of the forecasted power and load profiles were not considered and instead modeled linearly. The time interval was also set too low for real-life forecasting scenarios, and, as such, the time required to solve such an optimization problem for the ESS was higher than the set time. A smart residential energy management system was proposed in [20], where an artificial neural network (ANN) was utilized as a forecaster, and reinforcement learning (RL) was used to optimize ESS usage and overall ESS health by adjusting the loads between the grid or ESSs, as well as to determine the optimal battery action, namely, charge, discharge, and hold. Although this method reduces the dependency of the residential load on the grid, the methods used for such a model are time-consuming for practical deployment. Moreover, the paper did not consider an algorithm for diesel generators (DG). The work done in [21] showed that an LSTM neural network model outperformed the supervised feed-forward multilayer perceptron (MLP) model. In [22], machine learning-based PV power generation forecasting was explored based on a dataset from Alice Springs, Australia. The study showed that Random Forest regression performed better than Linear Regression, Polynomial Regression, Decision Tree Regression, SVM, LSTM, and MLP.

The results of [21] and [22] could not be compared because two different LSTM structures were used. In [23], the authors implemented an EMS with marginal degradation cost for the ESS. It was shown that implementing SOH constraints on EMSs increases the system's, thereby reducing the overall operational costs of the plant. Table 1 compares the methodologies of the referenced studies with those of the proposed designs.

While some of the aforementioned studies considered hybrid plants, power and load profile forecasting, and complex yet effective optimization methods, none considered a PV-DG-ESS hybrid plant with SOH constraints, accurate and time-feasible forecasting, or feedback correction. This study presents an Energy Dispatch Engine (EDE) that can overcome the previously stated research gap.

The proposed EDE model is a two-step controller, where short-term scheduling occurs during the first step, and corrections to the proposed schedule in the very short term occur during the second step. As shown in Table 1, this paper's contributions can be summarized as follows:

- A real-time two-stage MILP-based EDE governs a PV-DG-ESS hybrid plant utilizing accurate load, RES power, and cost forecasts using an LSTM neural network.
- Incorporating SOH and SOC constraints to reduce battery degradation and carbon emission cost constraints to reduce the carbon footprint.
- Employ active scheduling corrections during very short-term predictions using a feedback correction loop.
- The system was evaluated by benchmarking it against multiple systems [15].

The remainder of this paper is organized as follows: Section II details the methodology and modeling of the proposed EDE; Section III presents the system analysis and simulation results, and Section IV concludes the paper.

II. ENERGY DISPATCH ENGINE

A. DESIGN METHODOLOGY

An energy-dispatch-engine in operation is shown in Fig. 1. Typically, the ESS, RES, and grid are connected through a DC bus using DC–DC and AC–DC converters. In this configuration, the ESS can be charged through the RES or the grid. The ESS can also discharge power to loads or the grid.

The proposed EDE aims to maximize the profits of hybrid plants and the use of RESs and ESSs. The data analysis stage acquires data from the ESS (SoC, SoH, etc.) and diesel generators (generated power, aux. power), grid (past load data and profile), and RES (PV power) stations.

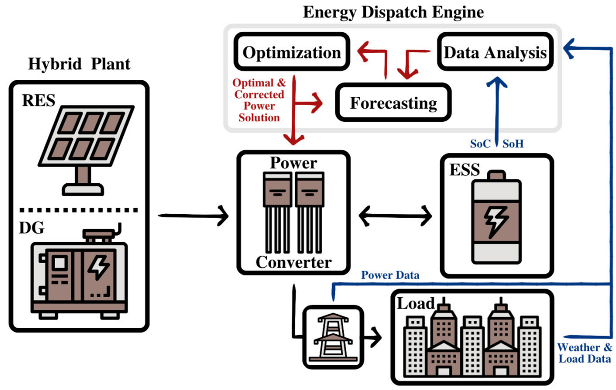

FIGURE 1. EDE-controlled hybrid plant.

The data are then bundled into data packets and prepared for forecasting and optimization. The optimal operation of the EDE follows three main processes found in any EMS, as illustrated in Fig. 1. As the accuracy of the EMS depends on the accuracy of the load and RES profile forecasting, the proposed design focuses heavily on the accuracy of the forecasted data. The forecasting errors are inversely proportional to the data intervals [24], [25]. As such, the forecasted data consists of 24-hour long data with 15 mins intervals. Forecasting updates, accurate load data, and accurate clean energy data ensure the optimality of the proposed system. Accordingly, multiple forecasting methods were considered. The EDE utilizes the entire length of the forecasted data (96 data points) for the long-term planning of RES and ESS use while performing real-time optimizations depending on the current load and RES power profiles.

To account for uncertainties and errors due to forecasting, optimized scheduling is constantly updated at each sampling time using more accurate forecasts. MILP was utilized to determine the optimal values for a given set of forecasts. As shown in Fig. 1, the system uses forecast and real loads, PV, and cost data.

B. FORECASTING

The data used to train and forecast the load and RES power profiles were gathered from Pecan Street data, used in [15], consisting of 1-minute PV power data and load data for 75 homes across the United States of America in 2018. The data were sampled down from its time-series form (size $2 \times n$, where n is the time series length) to 15-minute intervals and transformed into supervised-learning-appropriate data. The new dataset consists of 18 data points/features for the input, which break down into a day stamp (1-31), a month stamp (1-12), and 16 consecutive points in the PV/load time series, and 96 data points (representing 24 h sampled at 15 min) for the output, which is consecutive to the input. This arrangement, along with the large size of the data samples, ensures accurate day-to-day predictions considering the uncertainties and variations in load and PV generation.

TABLE 1. **EMS Methodology Comparison.**

System	Power Sources			Forecasting Method	Optimization Method	Constraints						Feedback Correction
	RES	DG	ESS			SOC	SOH	ESS	DG	RES	CO_2	
[12] [13]	✔	✔	✔	✘	Intra-Step MPC	✔	✘	✔	✔	✔	✔	Real-time
[14]	✔	✘	✔	✘	MPC	✔	✘	✔	✘	✔	✘	✘
[15]	✔	✘	✔	LSTM	Multi-stage Stochastic Model	✔	✘	✔	✘	✔	✘	Rule-Based
[16]	✔	✔	✔	✘	GA and Two-Point Estimate	✘	✘	✔	✔	✔	✘	✘
[17] [18]	✔	✔	✔	Markov-Reward Process	Markov-Reward Process	✘	✘	✔	✔	✔	✘	✘
[19]	✔	✘	✔	MPC	Multi-Layer MPC	✔	✔	✔	✘	✔	✘	MPC-Based
[20]	✔	✘	✔	ANN	RL	NA	✘	NA	NA	NA	✘	✘
[23]	✔	✘	✔	✘	Intertemporal Choice	✔	✔	✔	✘	✔	✘	✘
EDE	✔	✔	✔	LSTM	Two-Stage MILP	✔	✔	✔	✔	✔	✔	Real-time

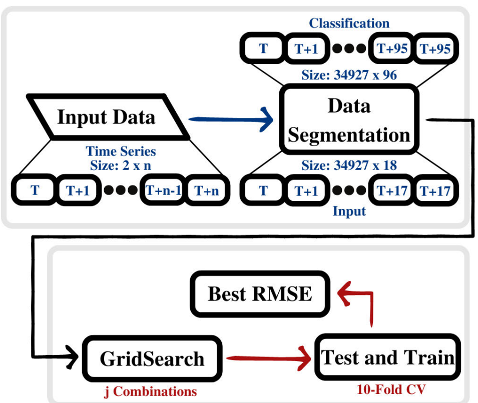

FIGURE 2. **Forecasting testing algorithm.**

All chosen algorithms were evaluated and compared based on their root mean square error (RMSE) values. A flowchart of the test is shown in Fig. 2. The test included training, testing, and validating each forecasting method multiple times using different hyperparameters over a 10-fold cross-validation to cover all seasons. The data were split using an 80:20 ratio for training and testing. The 10-fold cross-validation ensures that the trained model can accurately forecast data regardless of the time of year. The total number of combinations j was 116675000, and the tests were performed separately for both the PV and load data.

The SKlearn, SKforecast, and Keras libraries were used to construct the different algorithms. Table 2 summarizes the chosen ML methods and the total number of optimization iterations. Table 2 also shows the RMSE% results for all methods, whereas Figs. 3 and 4 show the top three test results for PV generation and load forecasting, respectively.

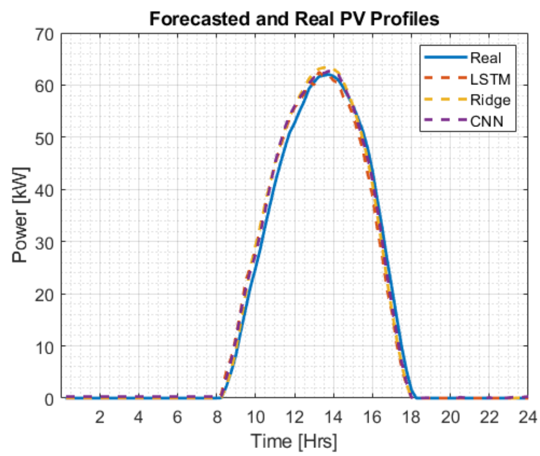

FIGURE 3. **Forecasted and real PV results.**

TABLE 2. **Forecasting Methods and Results.**

Model	Hyperparameters Iterations	Best RMSE %	
		PV	Load
LSTM	15000000	2.69	2.92
K-Ridge Regressor	6000000	2.98	3.56
CNN	15000000	3.29	5.32
Stochastic Model	12000000	3.52	6.21
SVM	8000000	4.19	8.60
Random Forest	60000000	4.23	9.01
K-Nearest Neighbor	675000	6.84	11.24

Table 2 lists the results for the chosen input size of 18 points (4 h from the past data). This number was chosen because it yielded the best (lowest RMSE%) among the values. The best RMSE results were obtained using a stacked unidirectional

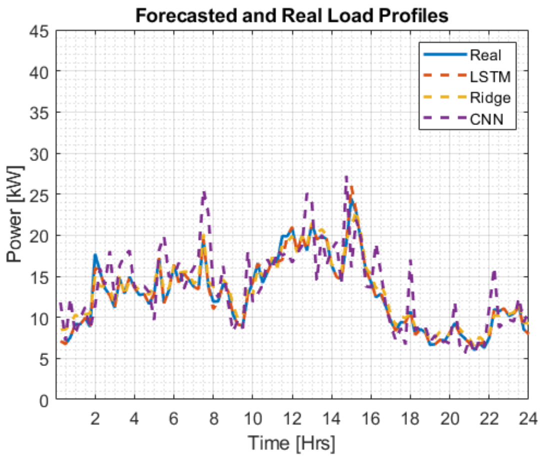

FIGURE 4. Forecasted and real load results.

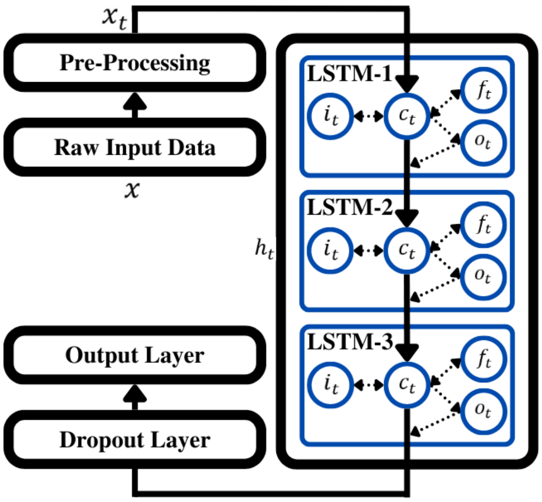

FIGURE 5. Forecasted and real load results.

LSTM architecture. This is because LSTM networks are structured using memory cells instead of neurons.

Single-layer LSTM models are simple and generally suitable for small time-series problems. A stacked bidirectional LSTM model would have performed better, as it captures dependencies in both the past and the future while still being capable of recognizing complex representations of the input data. As such, to achieve accurate results without being computationally extensive, a stacked unidirectional LSTM model was used, due to its ability to capture more complex patterns, such as those found in load and PV datasets. However, the proposed model lacks the ability to retain dependencies in both the past and the future. Mathematically, the proposed LSTM cells can be modeled as

$$f_t = \sigma(U_f x_t + W_f H_{t-1} + b_f) \tag{1}$$

$$i_i = \sigma\,(U_i x_t + W_i H_{t-1} + b_i) \tag{2}$$

$$u_i = \tanh(U_u x_t + W_u H_{t-1} + b_u) \tag{3}$$

$$c_t = (f_t \times C_{t-1}) + (i_t \times u_t) \tag{4}$$

$$\sigma_t = \sigma(U_o x_t + W_o H_{t-1} + b_o) \tag{5}$$

$$h_t = o_t \times \tanh\,(c_t) \tag{6}$$

where c_t is the memory cell, f_t is the forget gate, o_t is the output gate, x_t represents the input data, h_t is the hidden layer state, U and W are the matrix weights, b is the bias, and σ is the sigmoid function. Fig. 5 shows the developed LSTM architecture consisting of three stacked LSTM Layers. The significance of the bias b is to prevent overfitting, as well as improve the proposed models' ability to generalize new data. Adjusting the bias controls the amount of preserved load and PV data, which is useful for learning long-term dependencies and making the model more robust toward noise and data anomalies. This resulted in more accurate forecasts.

By contrast, the CNN model consists of three hidden layers using dilated convolution techniques. This was performed to accommodate the 1-D nature of the input data.

This result was also reflected in the CNN and LSTM results, where the LSTM results were 82% lower than the CNN results (PV forecasting) and 55% lower than the CNN results (load forecasting). It can also be observed that the load forecasting results were less accurate than the PV forecasting results. This is because of the shape of both the signals, where the PV data are smooth and have a small rate of change (fewer sharp changes), unlike the load data. These results match those in [14] and [20]. The cost was forecasted using the same LSTM algorithm.

C. PROBLEM FORMULATION

As stated, this energy dispatch engine aims to maximize the plant's profit and use RESs. Each element related to the previous statement should be formalized to achieve such results, and the objective stated above is equivalent to minimizing the plant's operating cost, using non-renewable energy resources, and the cost of emissions. In other words, the objective function J_{Total}can be expressed as

$$J_{Total} = J_{ESS} + J_{Grid} + J_{DG} \tag{7}$$

where J_{ESS}, J_{Grid}, and J_{DG} are the cost functions for the ESS, grid, and DG. The weightage of different cost functions here is equal, as the model's main purpose is to minimize the plants' operating cost, and all the cost functions in (18) fall into the same objective and are equally important.

J_{ESS} is modeled as the costs of the purchased power minus the sold power concerning the charging and discharging efficiencies for each time segment Δ_t as in

$$J_{\text{ESS}} = \sum_{t=1}^{t+N} \Delta_t \left(C_{\text{pur}}\,(t)\,\eta_{\text{ESS}}^{\text{ch}} P_{\text{ESS}}^{\text{ch}}\,(t) - \frac{C_{\text{sold}}\,(t)\,P_{\text{ESS}}^{\text{dis}}\,(t)}{\eta_{\text{ESS}}^{\text{dis}}} \right) \tag{8}$$

where C_{pur} is the cost of buying power, C_{sold} is the cost of selling power, $\eta_{\text{ESS}}^{\text{ch}}$ and $\eta_{\text{ESS}}^{\text{dis}}$ are the ESS's charging and discharging efficiencies, respectively, and $P_{\text{ESS}}^{\text{ch}}\,(t)$ and $P_{\text{ESS}}^{\text{dis}}\,(t)$ are the charged and discharged ESS powers, respectively. $t + N$ represents the cumulative sum for any given time t, where N is the length of the forecasted rolling horizon.

J_{DG} is modeled as the summation of the cost of fuel required to produce sufficient energy to power the grid loads and the cost of the associated emissions. The primary greenhouse gases emitted by diesel fuel are carbon dioxide (CO_2), methane (CH_4), and nitrous oxide (N_2O). As CO_2 represents 99.4% of the total emissions, the remaining gases are neglected [23]. By knowing the gas masses associated with burning diesel fuel, the cost of emissions can be expressed as a function of fuel consumption, such as

$$J_{\text{DG}} = \sum_{t=1}^{t+N} \Delta_t \left(\frac{P_{DG}^{Gen}(t)F}{P_{\text{DG}}^{\max}} \left(C_{\text{Fuel}} + C_{\text{Em}}\alpha_{\text{CO2}}\right) \right) \tag{9}$$

where $P_{DG}^{Gen}(t)$ is the DG-generated power, which is defined as the difference between the grids' purchased and sold power ($P_{\text{pur}}(t)$ and $P_{\text{sold}}(t)$, respectively), $P_{\text{DG}}^{\max}$ is the maximum power produced by the diesel generator, C_{Fuel} is the cost of fuel per liter, α_{CO_2} and C_{Em} are the gas mass associated with burning fuel and the cost of said gases, respectively, and F is the amount of diesel used per kWh.

J_{Grid} is modeled as the cost of purchased power minus the cost of sold power for each time segment.

$$J_{Grid} = \sum\nolimits_{t=1}^{t+N} \Delta_t \left(C_{pur}(t)P_{pur}(t) - C_{sold}(t)P_{sold}(t)\right) \tag{10}$$

The objective function in (7) can then be simplified as

$$J_{\text{Total}} = \sum_{t=1}^{t+N} \Delta_t \left(\begin{array}{l} C_{\text{pur}}(t)\,\eta_{\text{ESS}}^{\text{ch}} P_{\text{ESS}}^{\text{ch}}(t) - \frac{C_{\text{sold}}(t)P_{\text{ESS}}^{\text{dis}}(t)}{\eta_{\text{ESS}}^{\text{dis}}} + \\ \frac{(P_{\text{pur}}(t)-P_{\text{sold}}(t))F}{P_{\text{DG}}^{\max}} \left(C_{\text{Fuel}} + C_{\text{Em}}\alpha_{\text{CO2}}\right) + \\ C_{\text{pur}}(t)P_{\text{pur}}(t) - C_{\text{sold}}(t)P_{\text{sold}}(t) \end{array} \right) \tag{11}$$

It can be noticed that there are four main variables in the objective function, namely $P_{pur}(t)$, $P_{sold}(t)$, $P_{ESS}^{ch}(t)$, and $P_{ESS}^{dis}(t)$. Accordingly, the objective function can be rewritten as

$$J_{Total} = \sum_{t=1}^{t+N} \Delta_t \left(\begin{array}{l} P_{\text{ESS}}^{\text{ch}}(t)\left(C_{\text{pur}}(t)\,\eta_{\text{ESS}}^{\text{ch}}\right) \\ +P_{\text{pur}}(t)\left(\frac{F(C_{\text{Fuel}}+C_{\text{Em}}\alpha_{\text{CO2}})}{P_{\text{DG}}^{\max}} + C_{\text{pur}}(t)\right) \\ -P_{\text{ESS}}^{\text{dis}}(t)\left(\frac{C_{\text{sold}}(t)}{\eta_{\text{ESS}}^{\text{dis}}}\right) \\ -P_{\text{sold}}(t)\left(\frac{F(C_{\text{Fuel}}+C_{\text{Em}}\alpha_{\text{CO2}})}{P_{\text{DG}}^{\max}} + C_{\text{sold}}(t)\right) \end{array} \right) \tag{12}$$

The proposed cost function is subject to multiple constraints governing the system's behavior. The first constraint set is the power balance constraint as

$$\begin{aligned} P_{\text{DG}}(t) + P_{\text{PV}}(t) + P_{\text{ESS}}^{\text{dis}}(t) + P_{\text{pur}}(t) \\ - P_{\text{ESS}}^{\text{ch}}(t) - P_{\text{sold}}(t) - P_{\text{Load}}(t) = 0 \end{aligned} \tag{13}$$

where $P_{\text{DG}}(t)$ is the measured generated power, $P_{\text{PV}}(t)$ is the forecasted solar power, and $P_{\text{Load}}(t)$ is the forecasted load power. This is set to ensure that no excess power is generated.

A second constraint is set to balance the SOC of the ESS during charging and discharging cycles as

$$SOC(t) = SOC(t-1) + \frac{\Delta_t \left(\eta_{\text{ESS}}^{\text{ch}} P_{\text{ESS}}^{\text{ch}}(t) - \frac{P_{\text{ESS}}^{\text{dis}}(t)}{\eta_{\text{ESS}}^{\text{dis}}}\right)}{Q_{\text{ESS}} SOH(t)} \tag{14}$$

$$SOH(t) = \alpha SOC(t-1) + \beta \tag{15}$$

where $SOC(t)$ and $SOH(t)$ are the current state of charge and the state of health, respectively. This constraint ensures that the next SOC state is governed by the change in SOC with respect to time.

The values of α and β are set to be the constants of a linear approximator of the SOH using the SOC and the Depth of Discharge [23], [26], [27], and Q_{ESS} is the maximum (rated) capacity of the ESS.

The third set of constraints was added to control the behavior of the charge/discharge profile of the ESS as

$$ESS_{con} = \begin{cases} x.P_{\text{ESS-min}}^{\text{ch}} \le P_{\text{ESS}}^{\text{ch}}(t) \le x.P_{\text{ESS-max}}^{\text{ch}} \\ y.P_{\text{ESS-min}}^{\text{dis}} \le P_{\text{ESS}}^{\text{dis}}(t) \le y.P_{\text{ESS-max}}^{\text{dis}} \\ SOC_{\min} \le SOC(t) \le SOC_{\max} \\ SOH_{\min} \le SOH(t) \le SOH_{\max} \\ x, y \in \{0, 1\} \\ y = 1 - x \end{cases} \tag{16}$$

where $P_{\text{ESS-min}}^{\text{ch}}$, $P_{\text{ESS-max}}^{\text{ch}}$, $P_{\text{ESS-min}}^{\text{dis}}$, and $P_{\text{ESS-max}}^{\text{dis}}$, are the maximum/minimum bounds of the ESS's charging and discharging power, respectively, and $SOC_{\min}$, $SOC_{\max}$, $SOH_{\min}$, and $SOH_{\max}$, are the maximum/minimum bounds of the SOC and SOH, respectively. The SOC constraint ensures minimum and maximum reserve levels, while the charging and discharging power constraints ensure the transmission safety of the ESS. The variables x and y are considered to be binary (integer) variables responsible for the either/or behavior of the charging/discharging cycles of the ESS.

The final set of constraints is related to the grid, where the grid power and the diesel generator power are bounded between maximum and minimum values to ensure the transmission safety of the grid, as

$$Grid_{\text{con}} = \begin{cases} 0 \le P_{\text{DG}}(t) \le P_{\text{DG}}^{\max} \\ P_{\text{Grid}}^{\min} \le P_{\text{pur}}(t) - P_{\text{sold}}(t) \le P_{\text{Grid}}^{\max} \end{cases} \tag{17}$$

Equation (18) represents the final optimization problem.

$$\begin{cases} \underset{P_{pur}(t),P_{sold}(t),P_{ESSS}^{ch}(t),P_{ESSS}^{dis}(t)}{|\min|} & J_{\text{Total}} \\ s.t & (13)-(17) \end{cases} \tag{18}$$

D. MIXED-INTEGER LINEAR PROGRAMMING

Mixed-integer linear programming is a mathematical optimization tool that finds the best possible solution for a given objective function with respect to a set of constraints. MILP problems can be solved using three different methods: tree search, cutting plane, and feasibility pump [28].

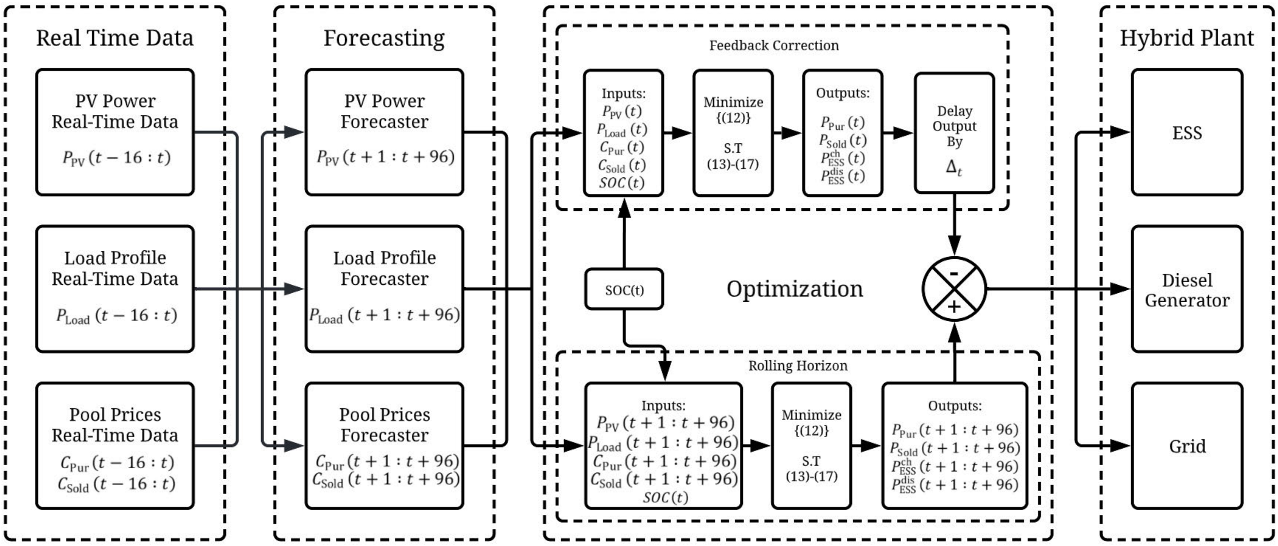

FIGURE 6. System Block Diagram With Optimization Algorithm Flowchart.

Because the proposed design utilizes the Gurbori optimization tool, the chosen MILP method is a tree search [29] that consists of three main stages: (1) the branching stage, where the problem is divided into two problems using a randomly chosen variable; (2) the bounding stage, where the branched problem is solved by finding the most optimal value for the chosen variable; and (3) the pruning stage, in which tree branching stops if the developed branch is infeasible [30].

The problem found in (18) was formulated based on MILP, and as such, it was written in the general MILP minimization format. The only integers are x and y, whereas $P_{pur}(t)$, $P_{sold}(t)$, $P_{ESS}^{ch}(t)$, and $P_{ESS}^{dis}(t)$are real variables.

MILP was chosen as the optimization method because of its high accuracy, considering its computational feasibility compared to other intelligent, metaheuristic, and classical methods [7].

TABLE 3. Simulation Parameters.

Constant	Value	Constant	Value
$\eta_{\mathrm{ESS}}^{\mathrm{ch}}$	0.90	Q_{ESS}	100 kWh
$\eta_{\mathrm{ESS}}^{\mathrm{dis}}$	0.85	C_{Fuel}	1.5 $/L
SOC_{min}	0.20	F	0.08 L/kW
SOC_{max}	0.90	$P_{\mathrm{DG}}^{\mathrm{max}}$	100 kW
SOC_{init}	0.50	$P_{\mathrm{Grid}}^{\mathrm{max}}$	100 kW
$P_{\mathrm{ESS-max}}^{\mathrm{ch}}$	40 kW	$P_{\mathrm{Grid}}^{\mathrm{min}}$	-60 kW
$P_{\mathrm{ESS-min}}^{\mathrm{ch}}$	0	C_{Em}	0.05 $/kg
$P_{\mathrm{ESS-max}}^{\mathrm{dis}}$	0	α_{CO2}	2.557 kg/L
$P_{\mathrm{ESS-min}}^{dis}$	-20 kW	SOH_{min}	0.70
Δ_t	15 min	SOH_{max}	0.99

E. FEEDBACK CORRECTION LOOP

To accommodate the forecasting errors and the non-uniform nature of errors in the forecasted data, a new 24-hour optimal schedule will be generated every 15 minutes. For any future values ($t > 0$), those newly generated schedules will not change. However, when the current time reaches a previously-scheduled time (or $t = 0$), real-time values of load, PV power, and SOC ($P_{\mathrm{Load}}(0)$, $P_{\mathrm{PV}}(0)$,and $SOC(0)$, respectively) will be the inputs of a parallel optimization loop that solves the same problem found in (18).

This optimization loop will decide the real-time (or $t = 0$) optimal sold and purchased power ($P_{\mathrm{Sold}}(t)$ and $P_{\mathrm{Pur}}(t)$ respectively), as well as the optimal ESS charge and discharge power ($P_{\mathrm{ESS}}^{\mathrm{ch}}(t)$ and $P_{\mathrm{ESS}}^{\mathrm{dis}}(t)$ respectively). This optimization loop's outputs are then subtracted from the previous optimized results from forecasted values, and corrections to the rolling horizon are made. This ensures accurate corrections to the scheduled rolling horizon to accommodate any sudden changes or deviations from the forecasted values.

III. SIMULATION RESULTS AND ANALYSIS

A. SIMULATION PARAMETERS

A Python library (CVXOPT) was used to solve the optimization problem. The system was tested and benchmarked against a heuristic model using the same parameters and a stochastic EMS model found in [15]. The heuristic model is a local search heuristic model, which follows a certain set of rules, and is similar to the heuristic model found in [15]. The ESS, in this case, charges when there is higher PV power than the load or at off-peak times, and discharges when the PV power is no longer sufficient.

The cost data were real-time sell/buy electricity pool prices sampled at 15-minute intervals. Table 3 presents the

TABLE 4. Optimization Results.

System	Evaluation Results ($/24h)	
	Daily Operational Cost	Daily CO_2 Emission Cost
EDE	42.91	6.55
Stochastic EMS [15]	44.35	N/A
Heuristic	47.27	9.28

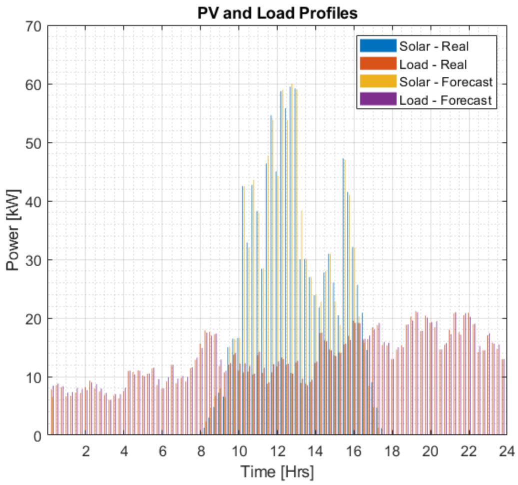

FIGURE 7. PV and load test data.

simulation parameters used in this study and the hybrid plants' parameters. The simulation uses real-time load, PV, and cost data, from the same Pecan Street Data dataset, for a later year. As such, the PV system is rated for 80 kW, the ESS has a maximum capacity of 100 kWh, and the DG can produce 100 kW.

Fig. 6 shows a general block diagram of the proposed algorithm and the optimization algorithm process. As shown in Fig. 6, the proposed model supports feedback correction in which the first step of the prediction horizon changes with time. This will help reduce the scheduling errors resulting from forecasting errors. It is also worth mentioning that forecaster training was periodically performed.

B. RESULTS AND ANALYSIS

Fig. 7–10 show the test results for both models. Fig. 7 represents the output of the forecasting stage, showing the forecasted PV and load profiles for the next 24-hours segment. In this case, the forecasted data starts and ends at midnight on two different days.

Fig. 8 shows the SOC% of the ESS throughout the day. It can be observed that the heuristic method utilizes the ESS only after sunset. This behavior is expected to change when the initial SOC% of the system is low, as it will only charge during off-peak hours and discharge during peak hours, leading to underutilization of the ESS. However, the

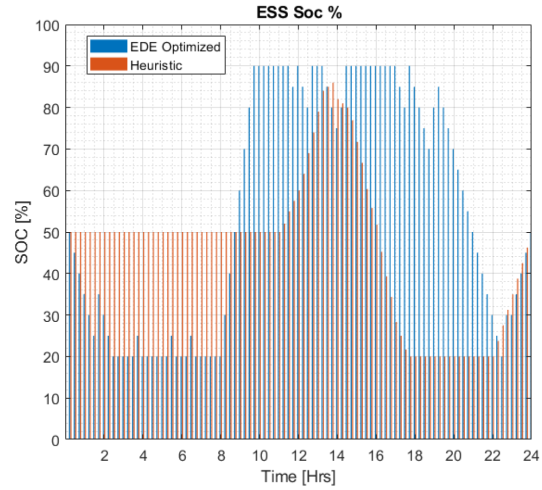

FIGURE 8. ESS SOC % comparison.

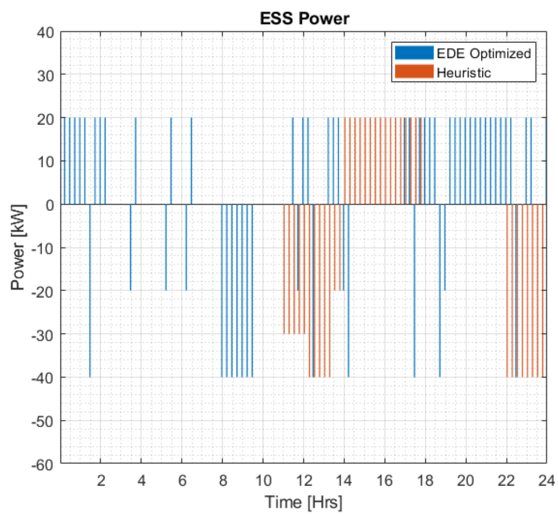

FIGURE 9. ESS power comparison.

proposed EMS fully utilizes the ESS during the day in terms of current and future power needs.

Fig. 9 shows the power flow of the ESS unit for both algorithms. As shown in Figs. 8 and 9, the EDE utilized an ESS with higher optimality than the heuristic method, where it was charged and discharged considering all given constraints and future power needs. By contrast, the heuristic system only charged the system when there was an influx of power and discharged it after sunset.

Fig. 10 shows the power consumed by or supplied to the grid. In the heuristic algorithm, the net grid power is positive and only experiences a dip when the PV system is active and ESS discharges. Unlike the heuristic algorithm, the net grid power in the proposed EDE algorithm experienced subtle fluctuations within the maximum and minimum power limits of the grid.

It can also be noticed that the net negative grid power in the proposed EDE is larger than the net negative grid power in the heuristic method (214.5 kWh and 149.4 kWh, respectively).

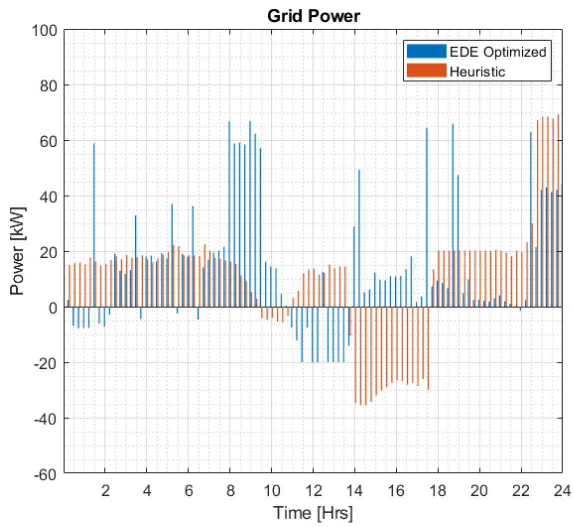

FIGURE 10. **Grid power comparison.**

This is because of ESS utilization by the proposed EDE. The system evaluation was related to the daily operational electricity and carbon emission costs, and the results are presented in Table 4. The rolling price of the heuristic method was higher than its EMS counterpart except during the sunset period.

The 24-hour electricity cost was 42.91$/24h for the EMS algorithm, 9.2% less than the heuristic method cost calculated at 47.27$/24h. Similarly, the daily CO_2 emission cost for the proposed EDE is 6.55$/24h, which is 29.4% less than the heuristic method CO_2 emission cost at 9.28$/24h.

The test results were also compared with the optimization method used in [15] with no daily CO_2 emission cost modification. Table 4 also lists the daily operational cost for the stochastic EMS in [15] as 44.35$/24h, 3.5% higher than the EDE optimized cost.

IV. CONCLUSION

Complicated ESS limitations, feedback correction, and load and solar power forecasting errors cause difficulties in the very short-term and short-term scheduling of hybrid plants. A two-stage MILP-based EDE was proposed in this study. The proposed model uses precise load and power forecasts, a feedback correction loop, and a set of constraints to control the SOC and SOH of the ESS and guarantee near-optimal scheduling. Such an EDE aims to reduce DG use and plant running expenses. Real-time load and PV data from 75 households were gathered and utilized with a PV-DG-ESS hybrid plant to assess the performance of the created model. The overall daily cost of the system was used as a metric to evaluate the system against a heuristic control model and multistage stochastic control model. Due to the forecasting technique, issue formulation, and feedback correction, the test results showed a 9.2% reduction in daily expenditures and a 29.4% reduction in CO2 emission costs compared with the heuristic control approach.

ACKNOWLEDGMENT

The findings achieved herein are solely the responsibility of the authors.

REFERENCES

[1] H. Hu, N. Xie, D. Fang, and X. Zhang, "The role of renewable energy consumption and commercial services trade in carbon dioxide reduction: Evidence from 25 developing countries," *Appl. Energy*, vol. 211, pp. 1229–1244, Feb. 2018, doi: 10.1016/j.apenergy.2017.12.019.

[2] H. Bevrani, M. Watanabe, and Y. Mitani, *Power System Monitoring and Control*. Hoboken, NJ, USA: Wiley, 2014.

[3] C. Sun, G. Joos, S. Q. Ali, J. N. Paquin, C. M. Rangel, F. A. Jajeh, I. Novickij, and F. Bouffard, "Design and real-time implementation of a centralized microgrid control system with rule-based dispatch and seamless transition function," *IEEE Trans. Ind. Appl.*, vol. 56, no. 3, pp. 3168–3177, May/Jun. 2020, doi: 10.1109/TIA.2020.2979790.

[4] W. Zhuo, A. V. Savkin, and K. Meng, "Decentralized optimal control of a microgrid with solar PV, BESS and thermostatically controlled loads," *Energies*, vol. 12, no. 11, p. 2111, Jun. 2019, doi: 10.3390/en12112111.

[5] J. Wang, K.-J. Li, Z. Javid, and Y. Sun, "Distributed optimal coordinated operation for distribution system with the integration of residential microgrids," *Appl. Sci.*, vol. 9, no. 10, p. 2136, May 2019, doi: 10.3390/app9102136.

[6] V. Veeramsetty, A. Mohnot, G. Singal, and S. R. Salkuti, "Short term active power load prediction on a 33/11 kV substation using regression models," *Energies*, vol. 14, no. 11, p. 2981, May 2021, doi: 10.3390/en14112981.

[7] J. Ma and X. Ma, "A review of forecasting algorithms and energy management strategies for microgrids," *Syst. Sci. Control Eng.*, vol. 6, no. 1, pp. 237–248, Jan. 2018, doi: 10.1080/21642583.2018.1480979.

[8] V. C. Onishi, C. H. Antunes, and J. P. F. Trovão, "Optimal energy and reserve market management in renewable microgrid-PEVs parking lot systems: V2G, demand response and sustainability costs," *Energies*, vol. 13, no. 8, p. 1884, Apr. 2020, doi: 10.3390/en13081884.

[9] E. O. Arwa and K. A. Folly, "Reinforcement learning techniques for optimal power control in grid-connected microgrids: A comprehensive review," *IEEE Access*, vol. 8, pp. 208992–209007, 2020.

[10] V. Khare, S. Nema, and P. Baredar, "Solar–wind hybrid renewable energy system: A review," *Renew. Sustain. Energy Rev.*, vol. 58, pp. 23–33, May 2016, doi: 10.1016/j.rser.2015.12.223.

[11] L. Moretti, M. Astolfi, C. Vergara, E. Macchi, J. I. Pérez-Arriaga, and G. Manzolini, "A design and dispatch optimization algorithm based on mixed integer linear programming for rural electrification," *Appl. Energy*, vols. 233–234, pp. 1104–1121, Jan. 2019, doi: 10.1016/j.apenergy.2018.09.194.

[12] M. S. Taha, H. H. Abdeltawab, and Y. A. I. Mohamed, "An online energy management system for a grid-connected hybrid energy source," *IEEE J. Emerg. Sel. Topics Power Electron.*, vol. 6, no. 4, pp. 2015–2030, Dec. 2018, doi: 10.1109/JESTPE.2018.2828803.

[13] B. Zhu, H. Tazvinga, and X. Xia, "Switched model predictive control for energy dispatching of a photovoltaic-diesel-battery hybrid power system," *IEEE Trans. Control Syst. Technol.*, vol. 23, no. 3, pp. 1229–1236, May 2015, doi: 10.1109/TCST.2014.2361800.

[14] D. Zhu and G. Hug, "Decomposed stochastic model predictive control for optimal dispatch of storage and generation," *IEEE Trans. Smart Grid*, vol. 5, no. 4, pp. 2044–2053, Jul. 2014.

[15] F. Hafiz, M. A. Awal, A. R. D. Queiroz, and I. Husain, "Real-time stochastic optimization of energy storage management using deep learning-based forecasts for residential PV applications," *IEEE Trans. Ind. Appl.*, vol. 56, no. 3, pp. 2216–2226, May 2020, doi: 10.1109/TIA.2020.2968534.

[16] S. S. Reddy and J. A. Momoh, "Realistic and transparent optimum scheduling strategy for hybrid power system," *IEEE Trans. Smart Grid*, vol. 6, no. 6, pp. 3114–3125, Nov. 2015, doi: 10.1109/TSG.2015.2406879.

[17] A. K. Barnes, J. C. Balda, and A. Escobar-Mejía, "A semi-Markov model for control of energy storage in utility grids and microgrids with PV generation," *IEEE Trans. Sustain. Energy*, vol. 6, no. 2, pp. 546–556, Apr. 2015, doi: 10.1109/TSTE.2015.2393353.

[18] J. Martins, S. V. Spataru, D. Sera, D.-I. Stroe, and A. Lashab, "Comparative study of ramp-rate control algorithms for PV with energy storage systems," *Energies*, vol. 12, no. 7, p. 1342, Apr. 2019, doi: 10.3390/en12071342.

[19] C. Ju, P. Wang, L. Goel, and Y. Xu, "A two-layer energy management system for microgrids with hybrid energy storage considering degradation costs," *IEEE Trans. Smart Grid*, vol. 9, no. 6, pp. 6047–6057, Nov. 2018, doi: 10.1109/TSG.2017.2703126.

[20] J. R. Wijesingha, B. V. D. R. Hasanthi, I. P. D. Wijegunasinghe, M. K. Perera, and K. T. M. U. Hemapala, "Smart residential energy management system (REMS) using machine learning," in *Proc. Int. Conf. Comput. Intell. Knowl. Economy (ICCIKE)*, Mar. 2021, pp. 90–95, doi: 10.1109/ICCIKE51210.2021.9410779.

[21] C. Liu, J. Gu, and M. Yang, "A simplified LSTM neural networks for one day-ahead solar power forecasting," *IEEE Access*, vol. 9, pp. 17174–17195, 2021, doi: 10.1109/ACCESS.2021.3053638.

[22] K. Mahmud, S. Azam, A. Karim, S. Zobaed, B. Shanmugam, and D. Mathur, "Machine learning based PV power generation forecasting in Alice springs," *IEEE Access*, vol. 9, pp. 46117–46128, 2021, doi: 10.1109/ACCESS.2021.3066494.

[23] G. He, S. Kar, J. Mohammadi, P. Moutis, and J. F. Whitacre, "Power system dispatch with marginal degradation cost of battery storage," *IEEE Trans. Power Syst.*, vol. 36, no. 4, pp. 3552–3562, Jul. 2021.

[24] M. Tan, S. Yuan, S. Li, Y. Su, H. Li, and F. He, "Ultra-short-term industrial power demand forecasting using LSTM based hybrid ensemble learning," *IEEE Trans. Power Syst.*, vol. 35, no. 4, pp. 2937–2948, Jul. 2020.

[25] F. Conte, F. D'Agostino, P. Pongiglione, M. Saviozzi, and F. Silvestro, "Mixed-integer algorithm for optimal dispatch of integrated PV-storage systems," *IEEE Trans. Ind. Appl.*, vol. 55, no. 1, pp. 238–247, Jan. 2019.

[26] L. Gustavsson and Å. Karlsson, "A system perspective on the heating of detached houses," *Energy Policy*, vol. 30, no. 7, pp. 553–574, Jun. 2002.

[27] S. Qu, Y. Kang, P. Gu, C. Zhang, and B. Duan, "A fast online state of health estimation method for lithium-ion batteries based on incremental capacity analysis," *Energies*, vol. 12, no. 17, p. 3333, Aug. 2019, doi: 10.3390/en12173333.

[28] J. P. Vielma, "Mixed integer linear programming formulation techniques," *SIAM Rev.*, vol. 57, no. 1, pp. 3–57, Jan. 2015.

[29] (2021). *Gurobi*. Accessed: Sep. 15, 2022. [Online]. Available: https://www.gurobi.com/resource/mip-basics/

[30] Z. C. Taşkin, "Tutorial guide to mixed-integer programming models and solution techniques," *Eng. Manag. Innov.*, pp. 521–548, Jan. 2008.

LAITH KANAAN (Graduate Student Member, IEEE) received the B.Sc. degree in electrical engineering from Qatar University, Qatar, in 2022. He is currently pursuing the M.Sc. degree in electrical engineering. He is a Research Assistant. His research interests include power electronics, renewable energy, microgrids, smart grids, V2G integration, intelligent and classical computational methods, efficient power transfer, pulsed-power applications, and high-power electromagnetics.

LOAY S. ISMAIL (Senior Member, IEEE) received the B.Sc. (Hons.) and M.Sc. degrees in electrical and computer engineering from Ain Shams University, Egypt, in 1990 and 1994, respectively, and the D.E.A. Diploma and Ph.D. degrees in informatics from Joseph Fourier University, Grenoble, France, in 1995 and 1999, respectively. He is currently an Academic Assessment Specialist and an Assistant Professor with the College of Engineering, Qatar University. He participated in a number of scientific research projects. He published more than 40 research and technical papers in the fields of the Internet of Things, wireless sensor networks, and multimedia documents authoring and presentation. His research interests include embedded systems, machine learning, and the Internet of Things.

SAMER GOWID (Senior Member, IEEE) received the B.Sc. degree in mechanical engineering from the Mechanical Engineering Department, Faculty of Engineering, Cairo University, Egypt, in 2001, and the Ph.D. degree in control systems engineering from the Wolfson School, Loughborough University, U.K., in 2017. He is currently a Lecturer in mechanical engineering with Qatar University, Qatar. His research interests include automation, control systems, fault diagnosis, artificial intelligence, smart farming, materials, and renewable energy.

NADER MESKIN (Senior Member, IEEE) received the B.Sc. degree from the Sharif University of Technology, Tehran, Iran, in 1998, the M.Sc. degree from the University of Tehran, Tehran, in 2001, and the Ph.D. degree in electrical and computer engineering from Concordia University, Montreal, QC, Canada, in 2008. He was a Postdoctoral Fellow with Texas A&M University at Qatar, from January 2010 to December 2010. He is currently a Professor with Qatar University, Doha, and an Adjunct Associate Professor with Concordia University. He has published more than 230 refereed journals and conference papers. His research interests include FDI, multiagent systems, active control for clinical pharmacology, cyber-security of industrial control systems, and linear parameter varying systems.

AHMED M. MASSOUD (Senior Member, IEEE) received the B.Sc. (Hons.) and M.Sc. degrees in electrical engineering from Alexandria University, Egypt, in 1997 and 2000, respectively, and the Ph.D. degree in electrical engineering from Heriot-Watt University, Edinburgh, U.K., in 2004. He is currently the Associate Dean for Research and Graduate Studies with the College of Engineering, Qatar University, Qatar, and a Professor with the Department of Electrical Engineering, College of Engineering, Qatar University. He supervised several M.Sc. and Ph.D. students with Qatar University. He has been awarded several research grants addressing research areas, such as energy storage systems, renewable energy sources, HVDC systems, electric vehicles, pulsed power applications, and power electronics for aerospace applications. He published more than 130 journal articles in the fields of power electronics, energy conversion, and power quality. He holds 12 U.S. patents. His research interests include power electronics, energy conversion, renewable energy, and power quality.